Doppler Imaging and Differential Rotation of 2 Coronae Borealis Using SONG*

The Astrophysical Journal, 893:164 (9pp), 2020 April 20 https://doi.org/10.3847/1538-4357/ab8229

Doppler Imaging and Differential Rotation of σ^2 Coronae Borealis Using SONG*

Yue Xiang[1,2], Shenghong Gu[1,2,3], A. Collier Cameron[4], J. R. Barnes[5], J. Christensen-Dalsgaard[6], F. Grundahl[6], V. Antoci[6], M. F. Andersen[6], and P. L. Pallé[7,8]

[1] Yunnan Observatories, Chinese Academy of Sciences, Kunming 650216, People's Republic of China; xy@ynao.ac.cn, shenghonggu@ynao.ac.cn
[2] Key Laboratory for the Structure and Evolution of Celestial Objects, Chinese Academy of Sciences, Kunming 650216, People's Republic of China
[3] School of Astronomy and Space Science, University of Chinese Academy of Sciences, Beijing 101408, People's Republic of China
[4] School of Physics and Astronomy, University of St. Andrews, Fife KY16 9SS, UK
[5] Department of Physical Sciences, The Open University, Walton Hall, Milton Keynes MK7 6AA, UK
[6] Stellar Astrophysics Centre (SAC), Department of Physics and Astronomy, Aarhus University, Ny Munkegade 120, DK-8000 Aarhus, Denmark
[7] Instituto de Astrofísica de Canarias, E-38205 La Laguna, Tenerife, Spain
[8] Departamento de Astrofísica, Universidad de La Laguna, E-38205 La Laguna, Tenerife, Spain

Received 2020 February 13; revised 2020 March 19; accepted 2020 March 19; published 2020 April 28

Abstract

We present new Doppler images of both components of the double-lined binary σ^2 CrB, based on the high-resolution spectroscopic data collected during 11 nights in 2015 March–April. The observed spectra form two independent data sets with sufficient phase coverage. We apply the least-squares deconvolution to all observed spectra to obtain high signal-to-noise mean profiles, from which we derive the Doppler images of both components of σ^2 CrB simultaneously. The surfaces of both F9 and G0 components are dominated by pronounced polar spots. The F9 component exhibits a weak spot at latitude 30° and its mid-to-low latitudes are relatively featureless. The G0 star shows an extended spot structure at latitude 30°, and its surface spot coverage is larger than that of the F9 star, which suggests a higher level of magnetic activity. With the cross-correlation method, we derive a solar-like surface differential rotation on the G0 star of σ^2 CrB for the first time, and the surface shear rate is $\Delta\Omega = 0.180 \pm 0.004$ rad days^{-1} and $\alpha = \Delta\Omega/\Omega_{\rm eq} = 0.032 \pm 0.001$. We do not obtain a clear surface shear law for the F9 star due to the lack of mid-to-low latitude features, but detect a systematic longitude shift of high-latitude spots, which indicates a slower rotation with respect to the corotating frame.

Unified Astronomy Thesaurus concepts: Stellar activity (1580); Close binary stars (254); Doppler imaging (400); Starspots (1572)

1. Introduction

Solar-like stars with a convection envelope show cool starspots caused by strong local magnetic field on stellar surfaces. Doppler imaging is a powerful technique for the study of spot activity on rapidly rotating stars. Recently, various active single and binary stars have been investigated by means of the Doppler imaging technique (Strassmeier 2009). Unlike that on the Sun, persistent large high-latitude or polar spots are detected on many active stars with different stellar parameters (e.g., Collier Cameron & Unruh 1994; Rice & Strassmeier 2001; Hackman et al. 2019). The magnetic flux is affected by dominant Coriolis force within the convection zone of rapid rotators to form high-latitude magnetic fields (Schüssler et al. 1996; Granzer et al. 2000). The rising magnetic flux-tube can also be affected by the tidal force to emerge at preferred longitudes (Holzwarth & Schüssler 2003), which are present on many active binary systems (e.g., Berdyugina et al. 1998; Olah 2006).

Differential rotation plays an important role in the stellar dynamo. Up to now, the solar-like latitude-dependent surface shear is detected on both single and binary stars, with the help of the Doppler imaging (e.g., Barnes et al. 2000; Dunstone et al. 2008; Kriskovics et al. 2014; Özdarcan et al. 2016). Some stars show anti-solar differential rotations (e.g., Kővári et al. 2007, 2017; Weber 2007; Harutyunyan et al. 2016), which means the equator rotates slower than the stellar pole. Gastine et al. (2014) suggested that the direction of differential rotation is determined by the Rossby number and the domination of the Coriolis force.

σ^2 CrB (TZ CrB, HD 146361, and HR 6063) is a component of the multiple system σ Coronae Borealis. Other components include a solar-like star σ^1 CrB and an M dwarf binary (Raghavan et al. 2009). σ^2 CrB is an active, double-lined binary, consisting of an F9 and a G0 stars, with an orbital period of about 1.14 day and an inclination degree of 28° (Strassmeier & Rice 2003; Raghavan et al. 2009). Both components of σ^2 CrB are young stars, which are on or close to zero main sequence. The components are very similar in mass, stellar radius, effective temperature, and evolutionary status (Strassmeier & Rice 2003).

Since both of the components are rapid rotators, σ^2 CrB is an ideal target for Doppler imaging and the two stars can be imaged simultaneously. Strassmeier & Rice (2003) presented the first Doppler images of both stellar components of σ^2 CrB, and revealed dominant cool polar spots as well as equatorial warm belts. The warm belt is located at the trailing hemisphere of each star with respect to the orbital motion. Donati et al. (1992) detected magnetic signatures for the G-type star from the Stokes V profiles, but did not for the F-type component. The Stokes V variations are mainly located in the profile core rather than in the wings, which suggests high-latitude magnetic field on the G-type component (Donati et al. 1992). The surface magnetic fields of both components were detected by Rosén et al. (2018) with the Zeeman–Doppler imaging technique, based on the polarization spectra data collected in 2014 and 2017, and the field strength of the G0 star is significantly stronger than that of the F9 star during their observing seasons.

* Based on observations made with the Hertzsprung SONG telescope operated on the Spanish Observatorio del Teide on the island of Tenerife by the Aarhus and Copenhagen Universities and by the Instituto de Astrofísica de Canarias.

Table 1
A Summary of Our Observations on σ^2 CrB in 2015

UT Start	UT End	No. of Frames	Exp. Time
03-27 23:49	03-28 06:18	39	600
03-31 23:02	04-01 06:13	39	600
04-02 22:57	04-03 06:17	44	600
04-04 22:35	04-05 03:10	28	600
04-06 23:58	04-07 04:48	29	600
04-08 22:19	04-09 06:10	47	600
04-10 22:41	04-11 06:00	44	600
04-11 22:07	04-12 06:05	12	600
04-12 23:22	04-13 06:02	33	600
04-14 00:13	04-14 00:33	3	600
04-14 22:46	04-15 05:55	43	600

We continued to monitor spot activity of a series of active binaries (Gu et al. 2003; Xiang et al. 2014, 2015, 2016, 2020). In this work, we present the Doppler images of both components of σ^2 CrB, based on the spectral data collected in 2015 March–April. We shall describe the observations and data reduction in Section 2. The surface images will be given and discussed in Sections 3 and 4, respectively. We shall summarize the final results in Section 5.

2. Observations and Data Reduction

High-resolution spectroscopic observations of σ^2 CrB were carried out with the 1 m Hertzsprung SONG telescope at the observatorio del Teide, Tenerife, Spain, from 2015 March 27 to April 15. Stellar Observations Network Group (SONG) plans to construct a global network of 1 m robotic telescopes, and the Hertzsprung SONG telescope is the first node (Andersen et al. 2014, 2019). The telescope is equipped with a high-resolution èchelle spectrograph (Grundahl et al. 2017). The resolution of the observed spectra is 75,000 and the coverage is 4400–6900 Å. For each frame, the exposure time was set to 600 s, which is corresponding to 0.6% of the rotational period of σ^2 CrB.

A total of 361 spectra were collected during the observing run. The 1D spectra were extracted with the SONG pipeline (Corsaro et al. 2012; Antoci et al. 2013). σ^2 CrB has a nearly integral-day period, which makes it difficult to observe effectively. We have observations of 11 nights, which are sufficient for two independent Doppler images. Thus these observed spectra were split into two data sets. One contains 179 spectra spanning from 2015 March 27 to April 7, and the other one contains 182 spectra spanning from 2015 April 8 to 15. Both data sets provide a very good phase coverage and dense sampling for the Doppler imaging of σ^2 CrB. The largest phase gap in the first data set is 0.04, and in the second data set is 0.05. We summarize the observations of σ^2 CrB of each night in 2015 in Table 1.

We applied the least-squares deconvolution (LSD; Donati et al. 1997) to combine all available atomic lines to obtain an average line profile with much higher signal-to-noise ratio. The stellar lines were extracted from the Vienna Atomic Line Database (VALD; Kupka et al. 1999) for a model atmosphere of $T_{\rm eff} = 6000$ K and $\log g = 4.5$. The values of $T_{\rm eff}$ and $\log g$ of σ^2 CrB are taken from Strassmeier & Rice (2003). The central wavelength and depth of spectral lines were used to create a line list that is required by the LSD computation. The lines within the regions of strong chromospheric (e.g., Na Double, H_α) and telluric lines were removed from the list. We also derived the deconvolved telluric line profiles from the observed spectra to estimate the instrument shifts in the wavelength calibration and corrected them (Collier Cameron 1999).

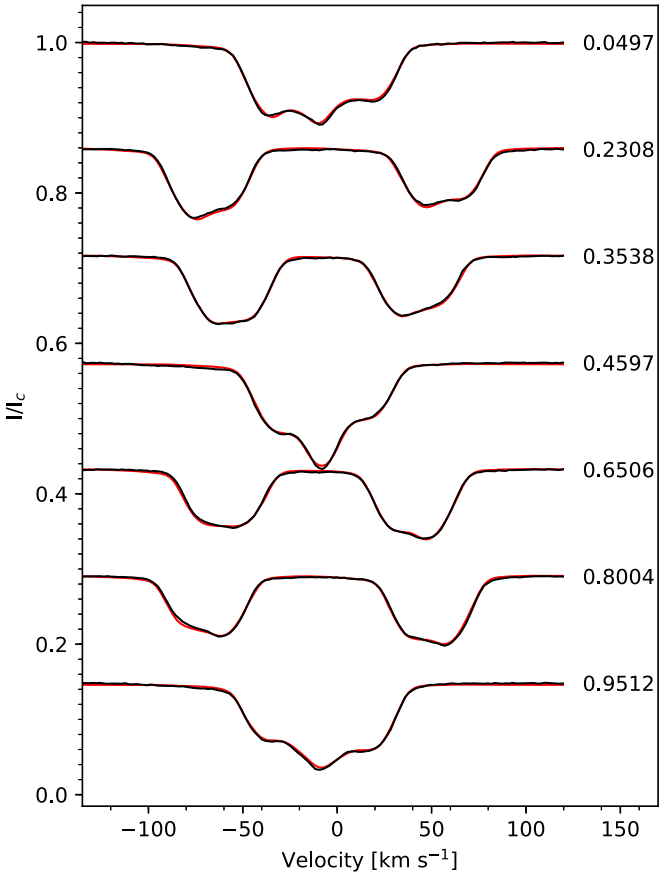

Figure 1. Examples of the observed (black) and the modeled (red) LSD profiles of σ^2 CrB. The rotational phase is annotated beside each profile.

We show examples of the resulting LSD profiles of σ^2 CrB and the corresponding modeled profiles in Figure 1. The line profiles of both components exhibit significant distortions, which indicates the presence of starspots on the two stars. We also show the phased time-series LSD profiles of two data sets in grayscale in Figure 2. In order to show spot signatures more clearly, an unspotted profile was subtracted from each observed profile. The time-series LSD profiles of the two components were dominated by strong signatures around the line center, which implies pronounced polar spots on the surfaces of both stars of σ^2 CrB.

Three inactive, slowly rotating template stars, HR 4540 (F9V), HR 4277 (G1V), and HR 5616 (K2III), were also observed with the same instrument setup during the observing run. Since our Doppler imaging code employs the two-temperature model, which treats the surface of a star as a combination of two components, hot photosphere, and cool spot, it requires a precalculated lookup table containing the local intensity of each component at each limb angle. Thus the spectra of template stars were deconvolved in the same manner to mimic the photospheres and spots of two stars. We used linear interpolation of the limb-darkening coefficients derived by Claret et al. (2012, 2013) for *UBVRI* passbands to obtain the values at the centroidal wavelength for the photosphere and

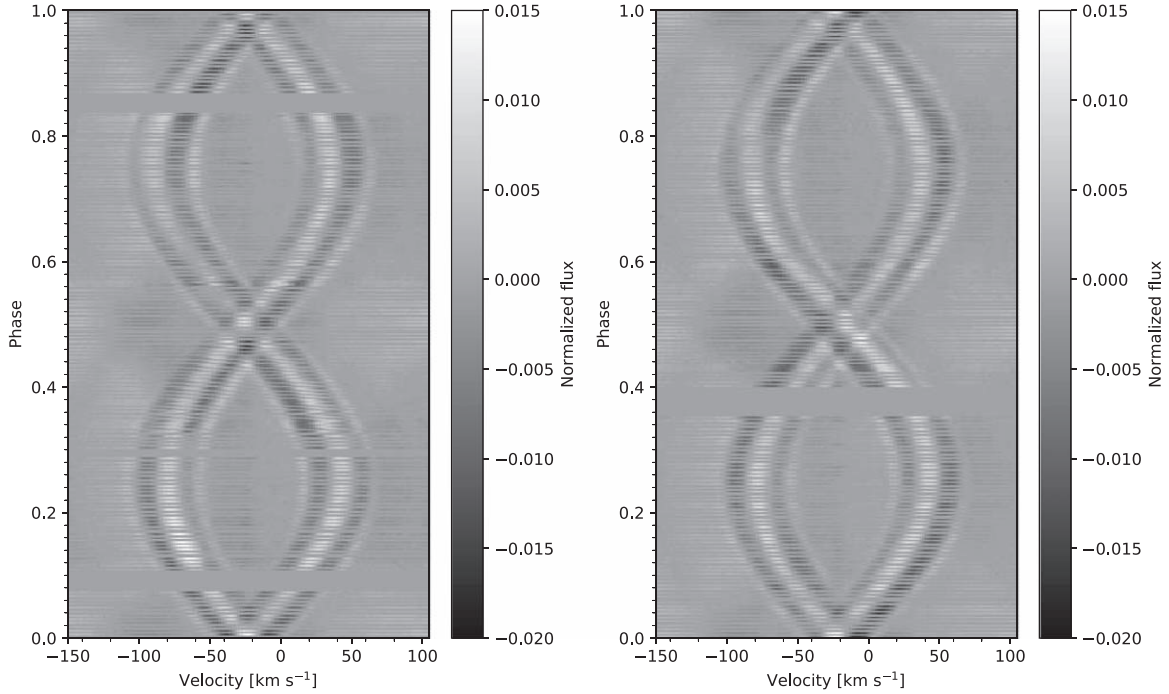

Figure 2. Phased time-series LSD profiles of the two data sets after subtraction of the unspotted profiles.

spot temperatures of each component star, and 30 limb angles were used for producing the lookup tables.

3. Doppler Imaging

3.1. Stellar Parameters

A reliable stellar surface reconstruction demands accurate system parameters, and errors in these parameters lead to spurious features (Collier Cameron & Unruh 1994). The parameters of σ^2 CrB have been well determined by Strassmeier & Rice (2003) and Rosén et al. (2018). Thus, in our case, we adopted the refined orbital elements, including the mass ratio (q), the radial velocity amplitudes of two stars (K), the inclination degree (i), the conjunction time (T_0), and the orbital period, derived by Rosén et al. (2018), and list them in Table 2. We fine-tuned the radial velocity of the mass center of the binary system (γ) with the χ^2 minimization method (Barnes et al. 2000), and the result is also shown in Table 2. Note that this value is the zero-point for our data set and not the true value, since we cannot determine the systematic instrument shift in our data sets without the radial velocity standard. We also tried to determine the projected equator rotational speed ($v \sin i$) through the same method. The result of both components is $v \sin i = 26$ km s^{-1}, which is in accordance with that derived by Strassmeier & Rice (2003).

Table 2
Adopted Stellar Parameters of σ^2 CrB for Doppler Imaging

Parameter	Value	Reference
$q = M_2/M_1$	0.9724	(a)
K_1 (km s^{-1})	61.366	(a)
K_2 (km s^{-1})	63.106	(a)
i (°)	28	(a)
γ (km s^{-1})	−12.4	DoTS
T_0 (HJD)	2450127.9054	(a)
Period (day)	1.13979045	(a)
$v \sin i_1$ (km s^{-1})	26	(b)
$v \sin i_2$ (km s^{-1})	26	(b)

Note. The F0 component is defined as the primary and the G0 star is the secondary.
References. (a) Rosén et al. (2018); (b) Strassmeier & Rice (2003).

3.2. Spot Images

We use the Doppler imaging code DoTS (short for DOppler Tomography of Stars) developed by Collier Cameron (1992, 1997) to perform the maximum entropy iterations to both data sets. The residuals between the observed LSD and modeled profiles were displayed in grayscale in Figure 3. Figure 4 shows the reconstructed surface images of the two components of σ^2 CrB. The mean spot filling factor as a function of latitude is plotted beside each image. Note that longitude 0° on the F9 star faces longitude 180° on the G0 star in our Doppler images. To show the relationship of the spot position on the surfaces of the two components of σ^2 CrB more clearly, we display 3D images of both components of σ^2 CrB at key orbital phases 0, 0.25, 0.5, and 0.75 for two data sets in Figures 5 and 6, respectively.

Our new Doppler images show a relatively simple spot pattern on the F-type component of σ^2 CrB. The main feature of the F9 star is a pronounced polar spot, which is consistent with what we see in the time-series LSD profiles (Figure 2). A very weak spot feature is present at both images of F9 star, but its longitude was changed from 300° to 270° during our observations. The surface of the G-type component of σ^2 CrB is also dominated by a polar spot, and it also shows an intermediate-latitude, extended spot structure between longitudes 30 and 210, connecting to the polar cap. The polar spot on each component is asymmetric with respect to the rotational axis, which is in good agreement with the results of Strassmeier & Rice (2003) and Rosén et al. (2018).

In order to determine the reliability of the surface features in our new Doppler images of σ^2 CrB, we also performed an odd–

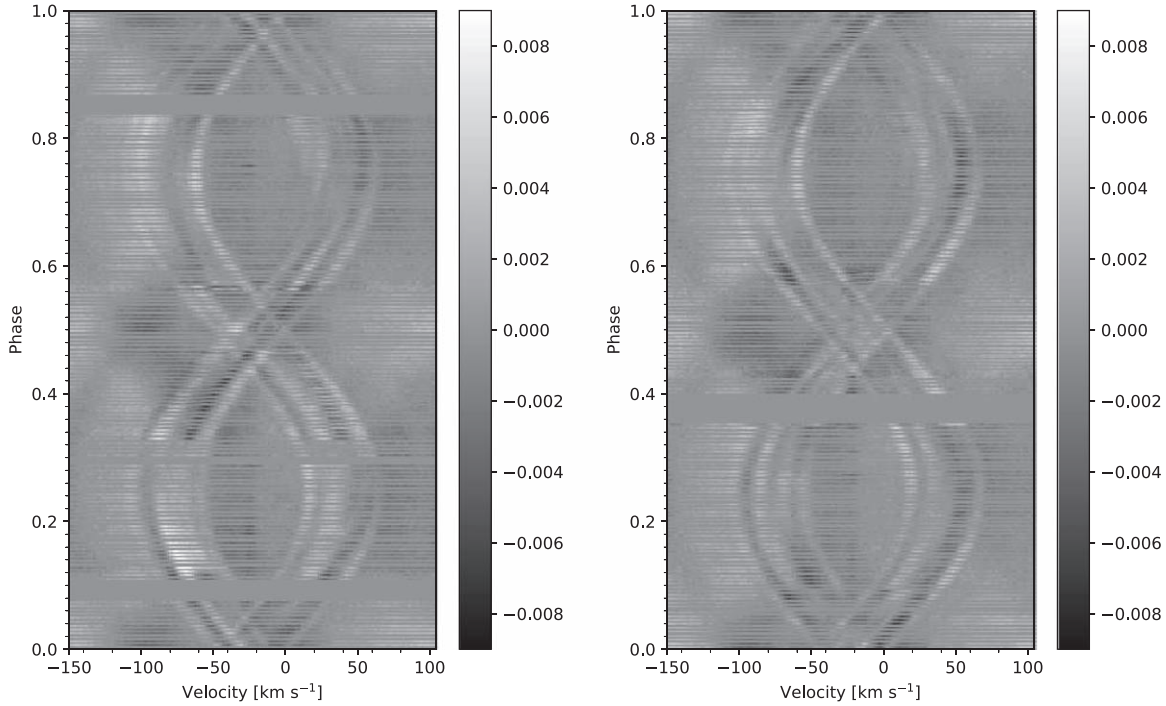

Figure 3. Residuals between the observed and modeled LSD profiles. White color means the observed data point is above the fit.

even test on the reconstructions. We split each data set into two subsets, which, respectively, consist of odd-numbered and even-numbered LSD profiles. Then we derived the surface images of the two components from the independent subsets. As shown in Figure 7, the reconstructed spot patterns in each image pair are nearly identical for each star, which demonstrates that our image reconstructions are reasonably reliable and that the dense sampling is helpful for the Doppler imaging.

3.3. Differential Rotation

The Doppler imaging can spatially resolve the stellar disk and thus can be used to measure the surface differential rotation. One can obtain the surface shear rate with either the cross-correlation (Donati & Collier Cameron 1997) or the image shear method (Petit et al. 2002). The cross-correlation method requires observations spanning at least two rotational cycles and good phase coverage. The advantage of this method is that it does not need any prior knowledge of the differential rotation law.

Two Doppler images several rotational periods apart may show a latitude-dependent rotation pattern. Actually, some clues can be seen directly from our Doppler images. The appendages of polar spots moved to less longitude between the two observation epochs, indicating a slower rotation of the high-latitude feature with respect to the corotating frame.

The first 39 spectra of data set No. 1 are collected on 2015 March 27, which is 4 days before the second observing night of 2015 March 31. This time interval is much larger than the rest and thus may introduce more errors in the estimate of the differential rotation. Hence, for the cross-correlation study, we first derived the Doppler images of the two components from data set No. 1 without the spectra of March 27. The new surface images are shown in Figure 8 and the phase coverage is still sufficient. Then we used these images and the ones derived from data set No. 2 to calculate the cross-correlation function of each latitude stripe on each component (Figure 9). The peak of the cross-correlation function of each latitude was determined by fitting a Gaussian profile. We tried to fit the peaks with a solar-like surface shear curve as follows

$$\Omega(l) = \Omega_{\rm eq} - \Delta\Omega \sin^2 l, \quad (1)$$

where l is the latitude and $\Omega_{\rm eq}$ is the rotational speed at equator and $\Delta\Omega$ is the difference between the equator and the stellar pole. The points between latitudes 20° and 70° were used, because the Doppler imaging technique has a poor longitude resolution at higher latitudes and is insensitive to the latitude of spots near the stellar equator, and latitudes below 20° were relatively featureless. The G0 component of σ^2 CrB shows a clear solar-like differential rotation, and the surface shear rate is $\Delta\Omega = 0.180 \pm 0.004$ rad days^{-1} and $\alpha = \Delta\Omega/\Omega_{\rm eq} = 0.032 \pm 0.001$. However, we failed to fit the cross-correlation map of the F9 component. It is probably due to that most spots on the F9 star are concentrated at high-latitude and no significant spot is present at mid-to-low latitudes.

4. Discussion

We have presented new Doppler images of both components of the double-lined binary σ^2 CrB, based on two data sets with very good phase coverage collected in 2015 March and April. The maximum entropy reconstructed images show that the surfaces of both components are dominated by pronounced polar spots. On each star, the polar spot is asymmetric with respect to the stellar pole. At latitude 30°, the G0 star also exhibits an extended spot structure connecting to the polar spot whereas the F9 star only shows a weak feature.

The epoch of our observations is just between two observing seasons of Rosén et al. (2018). The spot patterns in our surface images are compatible to their reconstructed brightness distributions, especially for high-latitude features. The polar

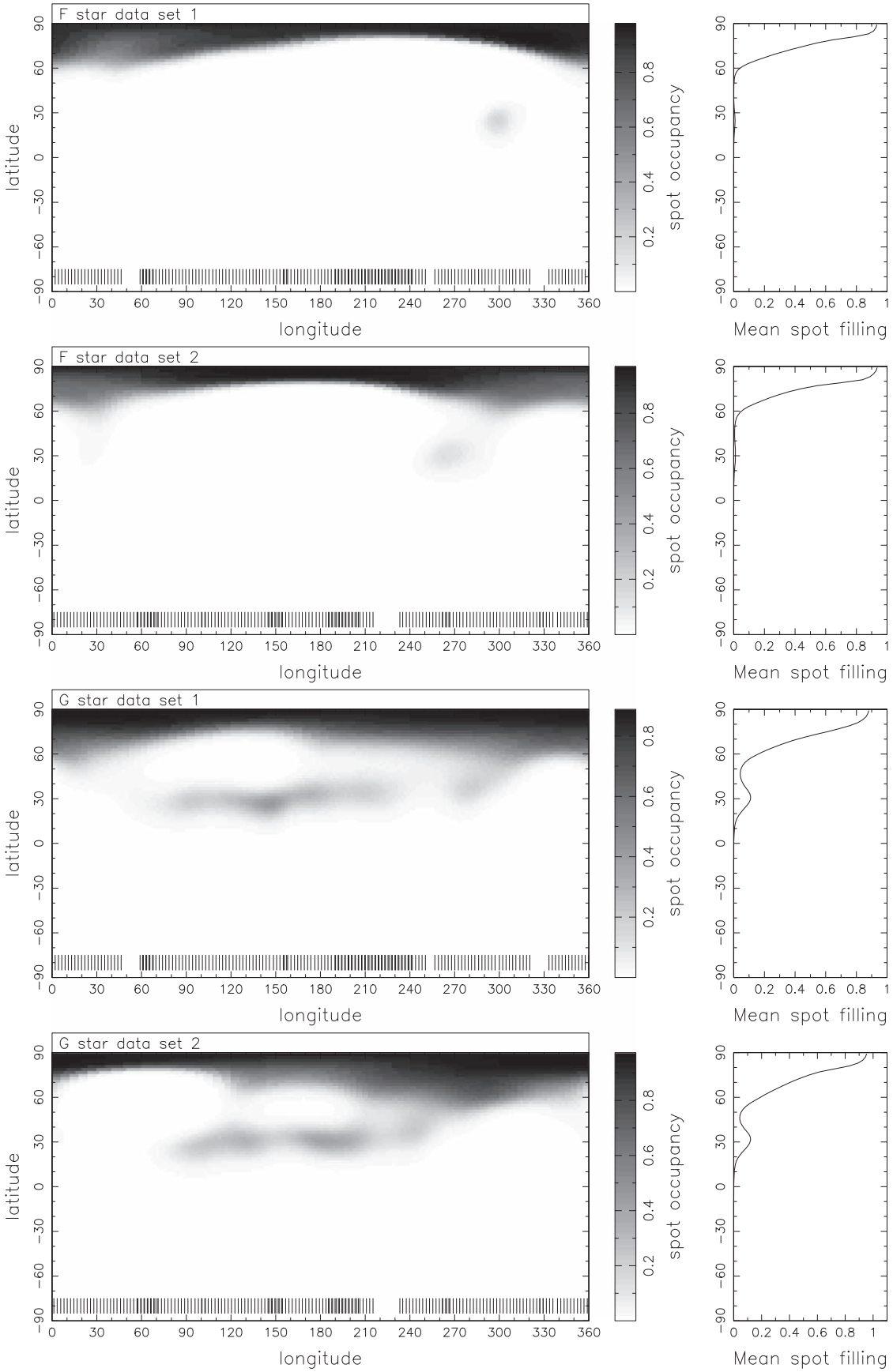

Figure 4. Doppler images of two stars. The observed phases are marked by the vertical ticks. The mean spot filling factor vs. latitude is plotted beside each image.

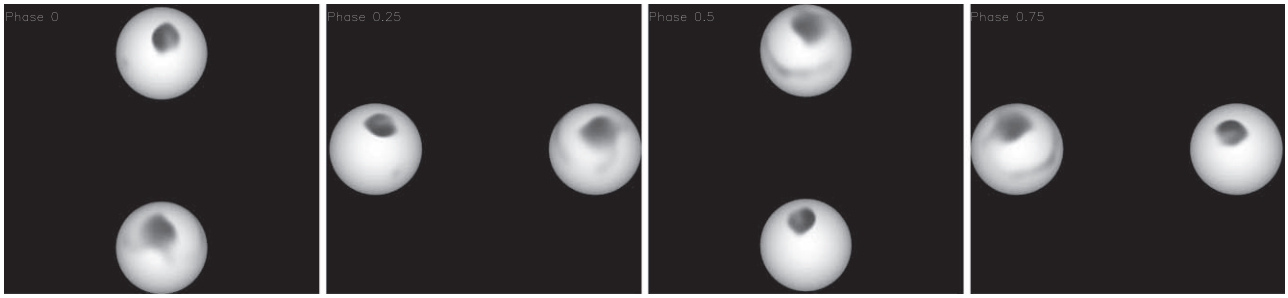

Figure 5. Images of the two components of σ^2 CrB, at phases 0, 0.25, 0.5, and 0.75, for data set No. 1.

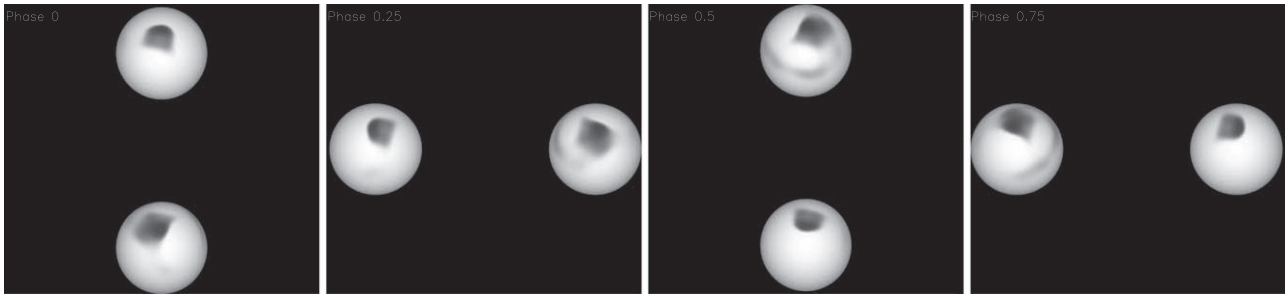

Figure 6. Same as Figure 5 but for data set No. 2.

spots on two components are revealed by all Doppler images. This may indicate a long lifetime for the polar spots on two stars, at least three years, which is common on active binaries (e.g., Strassmeier 2009). The spot configurations of mid-to-low latitudes in our images are different to those in their images, which should be due to the spot evolution.

Our Doppler images of the two components of σ^2 CrB are very compatible to those of Strassmeier & Rice (2003). They revealed the coexistence of dominant polar cool spots on both stars and the presence of a mid-to-high latitude cool spot on the F9 star. They also found an equatorial warm belt on the trailing hemisphere of each star with respect to the orbital motion. Since our Doppler imaging code uses the two-temperature model, we cannot reconstruct any hot spot on the stellar surface. The spot structure at latitude 30° on the G0 star is facing the F9 star, as seen in Figures 5 and 6. This is somewhat similar to the spot distribution of the two components of ER Vul (Xiang et al. 2015). However, considering the images of Rosén et al. (2018) in 2014 and 2017, the spot longitude distributions of both stars seem to be chaotic and they do not show any clear preferred active longitudes, which are found on many active binary and single stars (Strassmeier 2009). Apparently, any conclusive result on that requires more reproducible observations.

The spot coverages of the northern hemispheres of the F9 and G0 components of σ^2 CrB, derived from the reconstructed surface images, are 4.5% and 10.5%, respectively. The G0 star showed a higher level of spot activity than the F9 star in 2015. This difference is consistent with the results of Donati et al. (1992) and Rosén et al. (2018). Donati et al. (1992) only detected magnetic signatures on the G0 star but not on the F9 star, based on the polarization spectra data collected in 1990 and 1991. Rosén et al. (2018) modeled the Stokes V profiles of σ^2 CrB and detected magnetic field of both components, but the field strength on the G0 star is larger than that on the F9 star.

Considering the similarity of the two components of σ^2 CrB, it is interesting to see this persistent difference of magnetic activity levels of two stars in various observation seasons. The F9 and G0 stars have very close effective temperature, stellar mass, radius, and evolutionary status (Strassmeier & Rice 2003), which means that they should have similar depth of the convection envelope. The rotational periods of the two stars are equal to each other due to the tidal lock. These are believed to be the most important factors of the stellar dynamo, which generates magnetic field on stars. Rosén et al. (2018) inferred that the significant difference in magnetic field strengths of the two stars is not likely caused by their long-term activity cycle, because the same difference was also revealed by Donati et al. (1992) in 1990–1991 and it seems to be persistent for 30 yr, and that the strength difference is probably related to the different regimes of the stellar dynamo with low Rossby numbers, which can produce either a strong, dipole magnetic field or a weak, complex field on stars as revealed by Gastine et al. (2013).

The two solar-like components (G0V + G2V) of ER Vul are very similar to those of σ^2 CrB. The rotational period of ER Vul is 0.7 days, shorter than that of σ^2 CrB. Piskunov et al. (2001) presented the Doppler images of both components of ER Vul and found large temperature variations and the presence of hot spots at substellar points on the two stars. In our previous work (Xiang et al. 2015), we also derived Doppler images of ER Vul for 2006 and 2008 observing seasons. The spot patterns are more complex than those on σ^2 CrB. Both components of ER Vul show spots at various latitudes, from the equator to the stellar pole, and most mid-to-low latitude spots are concentrated at the hemisphere facing another star.

Another similar star is AF Lep, which is a single star with a similar spectral type (F8/9) and rotational period (1.0 day). The surface images derived by Järvinen et al. (2015) indicate the presence of a dominant high-latitude spot, similar to that on the F9 star of σ^2 CrB. Their theoretic models suggested that the radiative interior and the convection zone at the equator should have the same rotational speed to produce a high-latitude magnetic field.

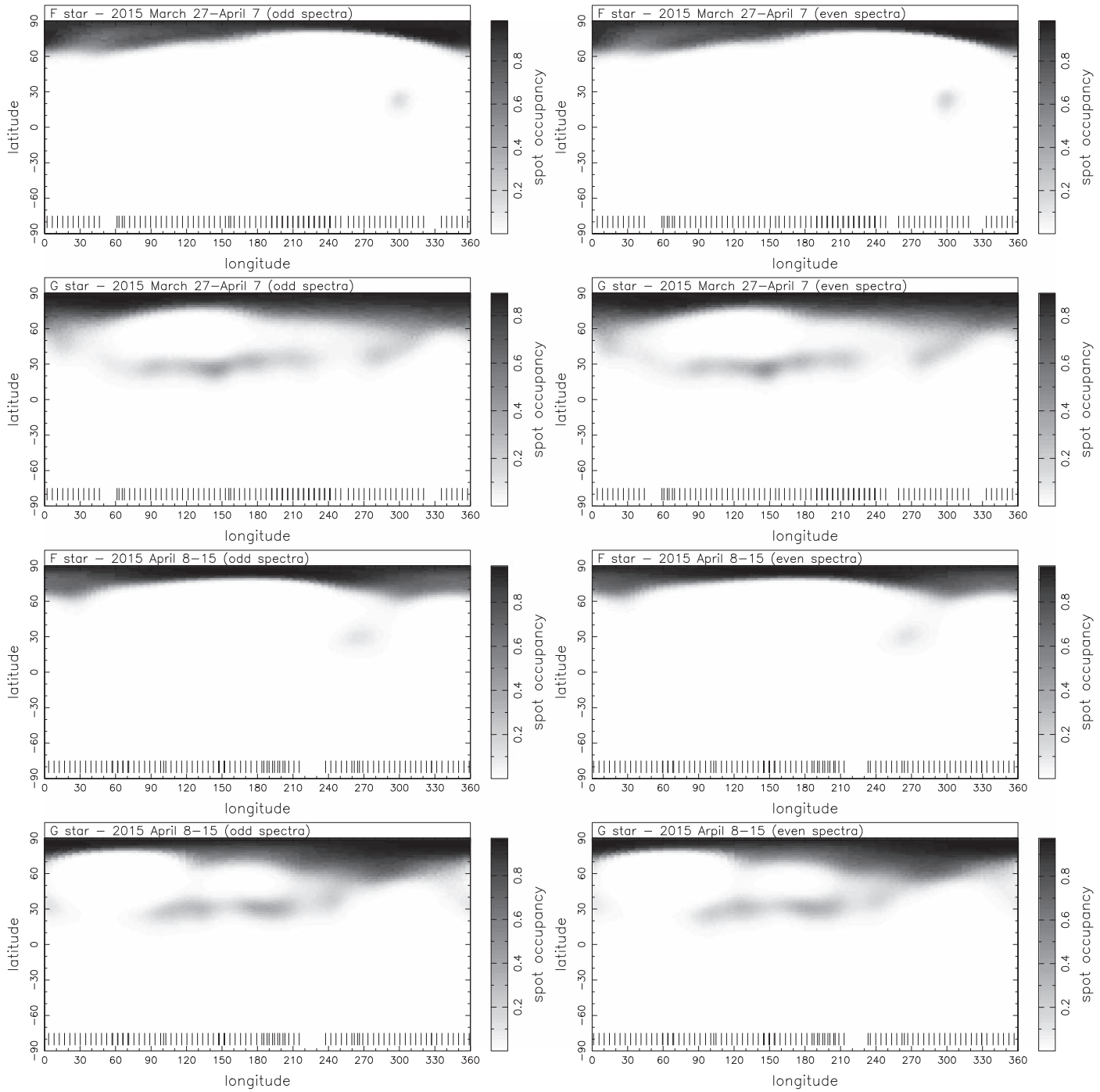

Figure 7. Doppler images of the two components derived from the odd-numbered and even-numbered spectra of two data sets.

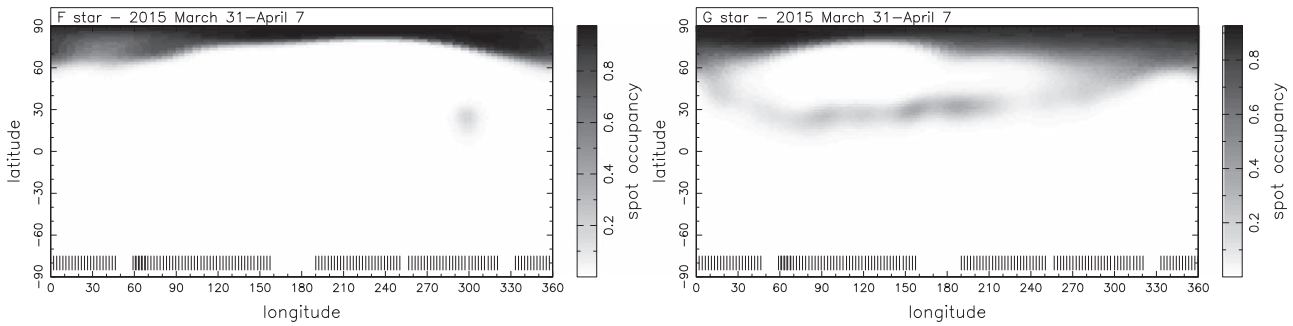

Figure 8. Doppler images of both components derived from data set No. 1 without observations in the night of 2015 March 27.

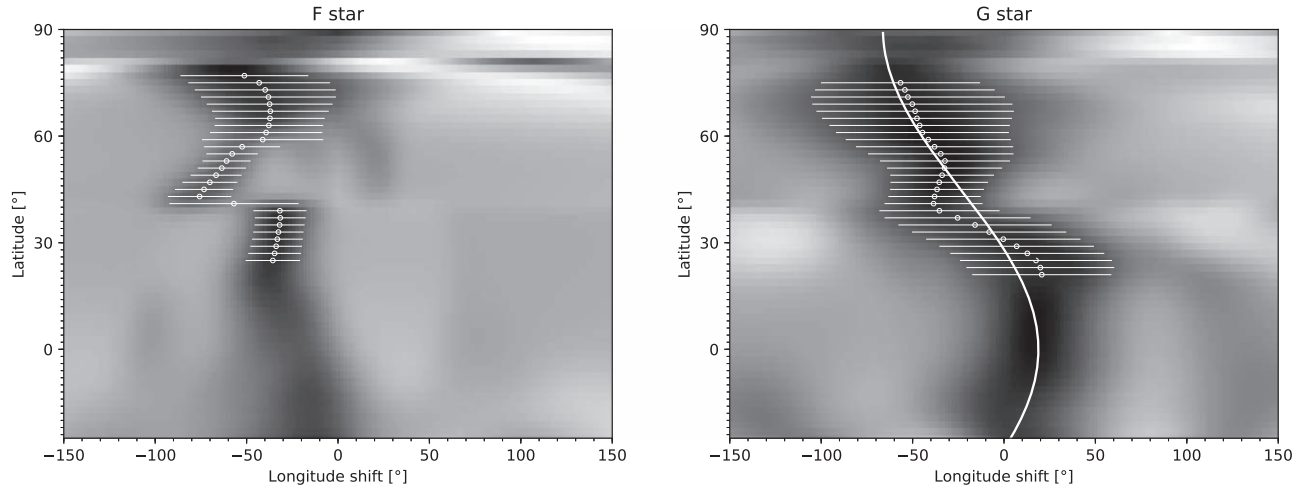

Figure 9. Cross-correlation maps of each latitude for the two components. The peak (white open circle) of the cross-correlation function for each latitude belt is determined by fitting a Gaussian profile and the full width at half maximum (FWHM) of the Gauss profile is presented by the white horizontal line. The white curve is a solar-like differential rotation fit.

A difference between the photometric and orbital periods was found by Strassmeier & Rice (2003) and Rosén et al. (2018). Rosén et al. (2018) estimated that the rotational periods of the F9 and G0 stars are 0.039 and 0.024 day longer than the orbital period. They attribute this to the surface differential rotation and the magnitude should be 0.1–0.19 rad day^{-1}. The larger rotational period may indicate that the dominant high-latitude features rotate more slowly than the orbital corotation (Rosén et al. 2018). The slower rotation of high-latitude features can be directly seen in our Doppler images. Although we cannot derive a clear differential rotation law for the F9 star due to the lack of mid-to-low latitude spots, we found that the high-latitude features were about 50° backward with respect to the corotating frame, corresponding to 6° per day. This is consistent with the estimate of Rosén et al. (2018).

Through the cross-correlation method, we derived a solar-like latitude-dependent rotation for the G0 star. The estimate is $\Delta\Omega = 0.180 \pm 0.004$ rad days^{-1}, which is in good agreement with the inference of Strassmeier & Rice (2003) and Rosén et al. (2018). The results indicate that the stellar equator of the G0 star rotates faster than the pole and laps it once every 35 days. Note that the error estimate is just statistical, and the spot evolution may induce more errors in the estimate of the surface shear, since our observing run spans 15 nights. Further multisite observations are needed to study the surface differential rotation of σ^2 CrB.

Recently, surface differential rotation on various single and binary stars has been detected, and the relationship between the surface shear rate and stellar parameters were investigated by many authors (Barnes et al. 2005; Collier Cameron 2007; Kővári et al. 2017). The surface differential rotation rate increases with the decrease of the depth of the stellar convection zone (Barnes et al. 2005; Marsden et al. 2011). The shear rate found on the G0 component of σ^2 CrB is in good agreement with the relations between the differential rotations and the effective temperatures derived by Barnes et al. (2005).

5. Conclusion

We obtained spectra of the double-lined binary σ^2 CrB with the 1 m Hertzsprung SONG telescope during 11 nights in 2015 March and April. The time-series LSD profiles derived from the observed spectra formed two independent, well-sampled data sets from which we derived two Doppler images of each component of σ^2 CrB.

Our new Doppler images show dominant polar spots on both of the F9 and G0 star components of σ^2 CrB, similar to those derived by Strassmeier & Rice (2003) and Rosén et al. (2018). These polar spots are asymmetric about the stellar rotational pole. The spot images also show a weak feature at intermediate latitude on the F9 star and an extended spot structure on the G0 star. The spot coverage of the G0 star is larger than that of the F9 star, which may indicate that the G star had a higher level of the magnetic activity than the F star during our observing seasons.

Differential rotation, as an important ingredient in generating stellar magnetic field, is difficult to quantify. The surface differential rotations of only tens of active stars have been measured by means of Doppler imaging, which can spatially resolve the stellar disk. These measurements require relatively long time-span observations covering several rotational cycles and sufficient phase sampling. Differential rotation rates of a variety of stars are needed to investigate the relations to the stellar parameters, such as the rotational periods and effective temperatures, to better understand the stellar dynamo.

The cross-correlation of latitude stripes of two independent Doppler images of the G0 star reveals a solar-like surface differential rotation. The shear rate is $\Delta\Omega = 0.180 \pm 0.004$ rad days^{-1}, which means the equator of the G0 star rotates faster than the stellar pole and laps it once every 35 days. The relative differential rotation rate of the G0 star is $\alpha = \Delta\Omega/\Omega_{\rm eq} = 0.032 \pm 0.001$. The cross-correlation map for the F9 star, however, does not show a clear differential rotation law, due to the lack of mid-to-low latitude features, but its high-latitude spots rotate slower with respect to the corotating frame.

The near 1 day period of σ^2 CrB makes it difficult to obtain complete phase coverage at only one site. In the future, with more spectroscopy telescopes of the SONG network at global sites, active stars with such integral-day rotational periods will be observed more effectively. This will greatly help us investigate their starspot activity and surface differential rotation.

This work is supported by National Natural Science Foundation of China (grant Nos. 10373023, 10773027, 11333006, 11603068, and U1531121) and Chinese Academy of Sciences project (No. KJCX2-YW-T24). Funding for the Stellar Astrophysics Centre is provided by The Danish National Research Foundation (Grant DNRF106). A special thanks goes to Antonio Pimienta and the team of operators at Observatorio del Teide who have contributed to the maintenance and running of the Hertzsprung SONG Telescope. We are very grateful to the anonymous referee for valuable comments and suggestions that significantly improved the clarity and quality of this paper. This work has made use of the VALD database, operated at Uppsala University, the Institute of Astronomy RAS in Moscow, and the University of Vienna.

ORCID iDs

Yue Xiang https://orcid.org/0000-0001-6580-9378
A. Collier Cameron https://orcid.org/0000-0002-8863-7828
J. Christensen-Dalsgaard https://orcid.org/0000-0001-5137-0966
F. Grundahl https://orcid.org/0000-0002-8736-1639
V. Antoci https://orcid.org/0000-0002-0865-3650

References

Andersen, M. F., Grundahl, F., Christensen-Dalsgaard, J., et al. 2014, RMxAC, 45, 83
Andersen, M. F., Handberg, R., Weiss, E., et al. 2019, PASP, 131, 045003
Antoci, V., Handler, G., Grundahl, F., et al. 2013, MNRAS, 435, 1563
Barnes, J. R., Collier Cameron, A., Donati, J.-F., et al. 2005, MNRAS, 357, L1
Barnes, J. R., Collier Cameron, A., James, D. J., & Donati, J.-F. 2000, MNRAS, 314, 162
Berdyugina, S. V., Berdyugin, A. V., Ilyin, I., & Tuominen, I. 1998, A&A, 340, 437
Claret, A., Hauschildt, P. H., & Witte, S. 2012, A&A, 546, A14
Claret, A., Hauschildt, P. H., & Witte, S. 2013, A&A, 552, A16
Collier Cameron, A. 1992, LNP, 397, 33
Collier Cameron, A. 1997, MNRAS, 287, 556
Collier Cameron, A. 1999, in ASP Conf. Ser. 185, IAU Coll. 170: Precise Stellar Radial Velocities, ed. J. B. Hearnshaw & C. D. Scarfe (San Francisco, CA: ASP), 233
Collier Cameron, A. 2007, AN, 328, 1030
Collier Cameron, A., & Unruh, Y. C. 1994, MNRAS, 269, 814
Corsaro, E., Grundahl, F., Leccia, S., et al. 2012, A&A, 537, A9
Donati, J.-F., & Collier Cameron, A. 1997, MNRAS, 291, 1
Donati, J.-F., Semel, M., Carter, B. D., Rees, D. E., & Collier Cameron, A. 1997, MNRAS, 291, 658
Donati, J.-F., Semel, M., & Rees, D. E. 1992, A&A, 265, 669
Dunstone, N. J., Hussain, G. A. J., Collier Cameron, A., et al. 2008, MNRAS, 387, 1525
Gastine, T., Morin, J., Duarte, L., et al. 2013, A&A, 549, L5
Gastine, T., Yadav, R. K., Morin, J., Reiners, A., & Wicht, J. 2014, MNRAS, 438, L76
Granzer, T., Schüssler, M., Caligari, P., & Strassmeier, K. G. 2000, A&A, 355, 1087
Grundahl, F., Andersen, M. F., Christensen-Dalsgaard, J., et al. 2017, ApJ, 836, 142
Gu, S.-H., Tan, H.-S., Wang, X.-B., & Shan, H.-G. 2003, A&A, 405, 763
Hackman, T., Ilyin, I., Lehtinen, J. J., et al. 2019, A&A, 625, A79
Harutyunyan, G., Strassmeier, K. G., Künstler, A., Carroll, T. A., & Weber, M. 2016, A&A, 592, A117
Holzwarth, V., & Schüssler, M. 2003, A&A, 405, 303
Järvinen, S. P., Arlt, R., Hackman, T., et al. 2015, A&A, 574, A25
Kővári, Zs., Bartus, J., Strassmeier, K. G., et al. 2007, A&A, 474, 165
Kővári, Zs., Oláh, K., Kriskovics, L., et al. 2017, AN, 338, 903
Kriskovics, L., Kővári, Zs., Vida, K., Granzer, T., & Oláh, K. 2014, A&A, 571, A74
Kupka, F., Piskunov, N., Ryabchikova, T. A., Stempels, H. C., & Weiss, W. W. 1999, A&AS, 138, 119
Marsden, S. C., Jardine, M. M., Ramírez Vélez, J. C., et al. 2011, MNRAS, 413, 1939
Oláh, K. 2006, Ap&SS, 304, 145
Özdarcan, O., Carroll, T. A., Künstler, A., et al. 2016, A&A, 593, A123
Petit, P., Donati, J.-F., & Collier Cameron, A. 2002, MNRAS, 334, 374
Piskunov, N., Vincent, A., Duemmler, R., Ilyin, I., & Tuominen, I. 2001, in ASP Conf. Ser. 223, 11th Cambridge Workshop on Cool Stars, Stellar Systems and the Sun, ed. R. J. Garcia Lopez, R. Rebolo, & M. R. Zapaterio Osorio (San Francisco, CA: ASP), 1285
Raghavan, D., McAlister, H. A., Torres, G., et al. 2009, ApJ, 690, 394
Rice, J. B., & Strassmeier, K. G. 2001, A&A, 377, 264
Rosén, L., Kochukhov, O., Alecian, E., et al. 2018, A&A, 613, A60
Schüssler, M., Caligari, P., Ferriz-Mas, A., Solanki, S. K., & Stix, M. 1996, A&A, 314, 503
Strassmeier, K. G. 2009, A&ARv, 17, 251
Strassmeier, K. G., & Rice, J. B. 2003, A&A, 399, 315
Weber, M. 2007, AN, 328, 1075
Xiang, Y., Gu, S., Wolter, U., et al. 2020, MNRAS, 492, 3647
Xiang, Y., Gu, S.-H., Cameron, A. C., & Barnes, J. R. 2014, MNRAS, 438, 2307
Xiang, Y., Gu, S.-H., Cameron, A. C., & Barnes, J. R. 2015, MNRAS, 447, 567
Xiang, Y., Gu, S.-H., Cameron, A. C., Barnes, J. R., & Zhang, L.-Y. 2016, MNRAS, 456, 314